J. theor. Biol. (1998) **194,** 461–483
Article No. jt980766

A Continuum Analysis of the Chemotactic Signal Seen by *Dictyostelium discoideum*

JOHN C. DALLON*† AND HANS G. OTHMER‡

**Mathematics Institute, Warwick University, Coventry CV4 7AL, U.K. and*
‡*Department of Mathematics, University of Utah, Salt Lake City, UT* 84112, *U.S.A.*

(*Received on* 10 *December* 1997, *Accepted in revised form on* 11 *June* 1998)

We develop a mathematical model of cell-to-cell-signaling in *Dictyostelium discoideum* that predicts the cAMP signal seen by individual cells in early aggregation. The model employs two cells on a plane and is designed to predict the space–time characteristics of both the extracellular cAMP signal seen by one cell when a nearby cell relays, and the intracellular cAMP response produced by the stimulus in the receiving cell. The effect of membrane bound phosphodiesterase is studied and it is shown that cells can orient effectively even in its absence. Our results give a detailed picture of how the spatio-temporal characteristics of the extracellular signal can be transduced into a time- and space-dependent intracellular gradient, and they suggest a plausible mechanism for orientation in a natural chemotactic wave.

1. Introduction

In the vegetative phase, cells of the cellular slime mold *Dictyostelium discoideum* (Dd hereafter) live as individual amoebae, feed on bacteria, and multiply by binary fission (Bonner, 1982). After a period of starvation they become chemotactically sensitive to cycle adenosine 3′,5′-monophosphate (cAMP), and by 6 to 10 hours after the onset of starvation virtually all of the cells are relay competent (Gingle & Robertson, 1976). This means that cells can sense and move toward a source of cAMP, and they relay the signal as well by secreting cAMP. After about 8 hours of starvation, randomly-located cells called pacemakers begin to emit cAMP periodically (Raman *et al.*, 1976). Nearby cells move toward these pacemakers, but to do so, they must detect the composite signal received from the pacemaker and relaying neighbors and determine the direction of movement.

The transition from free-ranging amoeba to a multicellular fruiting body in Dd involves many of the basic processes, including chemotaxis and cell movement, that occur in other developing systems. Since cell movement plays a fundamental role in such diverse processes as embryonic development, the response of the immune system, and wound healing, a better understanding of cell movement in Dd will be valuable in a number of other contexts. However there are still many fundamental questions regarding cell movement that are unresolved, including the

† Author to whom correspondence should be addressed at: Department of Mathematics, Heriot-Watt University, Edinburgh EH14 4AS, U.K.

0022–5193/98/020461 + 23 $30.00/0

microscopic issues of how a cell decides when to move, how it determines the direction in which to move, and how long it moves. In a previous paper (Dallon & Othmer, 1997) we developed and analysed a discrete cell model for the aggregation of Dd which allowed us to explore the effect on macroscopic aggregation patterns of changes in the microscopic rules by which cells determine their direction and duration of movement. In this paper we focus on the microscopic cAMP environment which individual cells sense via the cAMP receptors on their surface. The purpose is to understand what features of the cAMP signal might be used for orientation of cells in a chemotactic wave.

Some form of directed or non-random cell movement is essential for aggregation, and leads to the question of whether, and if so how, cells can extract directional information from an extracellular field. In the case of flagellated bacteria such as *E. coli*, movement consists of a series of more-or-less straight runs, punctuated by tumbles during which a cell chooses a new direction. These bacteria move at a fixed speed, but they extend their run length when moving up the gradient of an attractant. Since they are small they probably cannot discriminate spatial differences in the concentration of an attractant on the scale of a cell length, and they simply choose a new direction more or less at random (Berg & Brown, 1972; Berg, 1975). The propensity of a flagellum to rotate clockwise or counterclockwise, and hence the probability of a run or tumble, is biased by an intracellular signal whose level is determined by inputs from all receptors, and thus reflects an average signal over the cell surface (Spiro *et al*., 1997). However, it is conceivable that larger cells such as Dd are able to extract directional information from the extracellular cAMP distribution. Since the cAMP distribution is a scalar field, directional information can only be obtained from this field by *effectively* taking measurements at two points in space, and the question is how this can be done?

In the absence of cAMP stimuli Dd cells extend pseudopods in random directions, perhaps for determining a favorable direction in which to move, and aggregation competent cells respond to cAMP stimuli with characteristic changes in their morphology. The first response is suppression of existing pseudopods and rounding up of the cell (the ''cringe response''), which occurs within about 20 seconds and lasts about 30 seconds (Condeelis *et al*., 1990). Under uniform elevation of the ambient cAMP this is followed by extension of pseudopods in various directions, and an increase in the motility (Varnum *et al*., 1985; Wessels *et al*., 1992). A localized application of cAMP elicits the cringe response followed by a localized extension of a pseudopod near the point of application of the stimulus (Swanson & Taylor, 1982). This type of stimulus is similar to what a cell experiences in a cAMP wave.

Cells also respond to static gradients of cAMP. Fisher *et al*. (1989) show that cells move faster up a cAMP gradient than down, and that the majority of turns made by a cell are spontaneous (although there is a slight depression in the frequency of turns when the cell moves up the gradient). However, the magnitude and direction of a turn is strongly influenced by the gradient in that there is a strong tendency to lock onto the gradient. Furthermore, aggregation is not affected by the absence of relay [treating cells with caffeine suppresses relay but does not impair their chemotactic ability (Brenner & Thomas, 1984; Siegert & Weijer, 1989)]. The ability of larger cells such as Dd to apparently ''measure'' concentration differences over the length of the cell body has led to the following proposals as to how this might be done:

- a spatial gradient sensing mechanism, in which the cell measures the concentration difference or the difference in the number of occupied receptors between front and back (Mato *et al*., 1975; Zigmond, 1978; McRobbie, 1986);
- the differential force mechanism, in which the strength of adhesion to the substrate or to other cells depends on the chemoattractant. In a macroscopic description of chemotaxis this leads to an expression for the chemotactic sensitivity in terms of the sensitivity of the force exerted as a function of the attractant concentration (Pate & Othmer, 1986; Othmer & Pate, 1987);

• the "pseudo-spatial" mechanism in which cells extend pseudopods and convert the spatial gradient in attractant sensed into a temporal rate of change of attractant (Gerisch *et al*., 1975a);

• a spatio-temporal threshold mechanism, in which the orientation is determined by an internal gradient that is created by the extracellular gradient of the attractant. If there is adaptation in the chemotactic signal transduction pathway, then the internal gradient will decay, even in the presence of a steady external gradient, unless cells move. Internal gradients are known to exist in newt eosinophils, where the development of a calcium gradient is necessary to cell polarization (Brundage *et al*., 1991; Gilbert *et al*., 1994).

Later we show that the last mechanism is feasible for orientation on the times scale necessary.

Previous theoretical analyses of signaling either ignore the membrane bound phosphodiesterase (mPDE) completely (Gerisch *et al*., 1975b; Rossier *et al*., 1980) or distribute the phosphodiesterase activity uniformly in space (Pate & Odell, 1981; Martiel & Goldbeter, 1987; Monk & Othmer, 1989; Tang & Othmer, 1994). Models of aggregation have also either ignored the mPDE (MacKay, 1978; Cohen & Robertson, 1971; Levine & Reynolds, 1991; Vasiev *et al*., 1994; Savill & Hogeweg, 1997), distribute the phosphodiesterase activity uniformly in space (Parnas & Segel, 1977; Höfer *et al*., 1995) or ignore the cAMP dynamics completely (Vasieva *et al*., 1994). While the approach of distributing the phosphodiesterase activity uniformly in space may represent the average rate of degradation adequately, it does not yield the detailed spatial distribution of attractant in the immediate neighborhood of a cell. These aggregation models and others (Oss *et al*., 1996; Dallon & Othmer, 1997) focus on pattern formation, and since the models describe the system from a macroscopic viewpoint they cannot address the detailed features of the chemotactic signal.

Early experimental support for the hypothesis that cells respond to the spatial gradient stems from the work of Mato *et al*. (1975). These authors used the chemotactic drop assay, in which drops of cAMP are placed near a droplet of cell suspension containing about 500 cells, and the distances at which 50% of the cells respond for a given cAMP concentration are measured. A log–log plot of the number of cAMP molecules vs. the threshold distance yields an approximately straight line in Mato *et al*.'s experiments, the best fit slope of which is 1/4.25. Theoretical analysis of the threshold relationship for diffusion from a point source in 3-D shows that the slope is 1/4 if the maximum spatial gradient triggers movement, and thus the authors interpret their experimental results to mean that cells probably respond to the spatial gradient. However, as was shown elsewhere, a slightly different analysis of their data could lead to the conclusion that a temporal sensing mechanism is operative (Othmer & Schaap, 1997).

Numerous other experiments (Futrelle *et al*., 1982; Swanson & Taylor, 1982; Fisher *et al*., 1989; Vicker, 1994) have been designed to determine which of the foregoing mechanisms are used to determine how to move, but the results are inconclusive, in part because the spatio-temporal characteristics of the signal seen by a cell are not known. Here we develop a mathematical model for signaling between two relay-competent cells based on a geometrically-realistic representation of the cells. The model treats the cells as objects with specified volumes and boundaries and accurately reflects the spatial and temporal scales in signaling and the spatial localization of key enzymes. Thus we believe that the solutions of the governing equations accurately reflect the spatial characteristics of the signal near the cell membrane, as well as in the cytoplasm. As a result, it would provide the level of detail necessary for understanding what aspects of the spatio-temporal signal can be used to orient a cell.

In addition this analysis may shed light on what mechanisms the cell could use to determine when to move and what constitutes a movement cycle. Recent experimental data suggest that cells do not choose new directions via a temporal Poisson process, which would be the case if the probability per unit time of extending a pseudopod were constant. Instead there appears to be an intrinsic periodicity to the extension of pseudopods, at least in unstimulated amoeba

(Killich *et al*., 1993; Shenderov & Sheetz, 1997). Furthermore, it has been suggested that Dd uses separate mechanisms for the control of orientation and cell movement (Van Duijn & Van Haastert, 1992). In Dallon & Othmer (1997) it was shown that an effective mechanism for determining when to move could be based on an intracellular signal that is determined by the extracellular signal averaged over the cell. However another mechanism is needed to determine the cell's orientation, some possible candidates for which were discussed above.

The analysis we present is deterministic in that we do not account for fluctuations in the number of molecules near a cell. While these are undoubtedly important at the level of receptor binding, the intracellular cAMP signal may be much less "noisy" because the receptor occupancy is integrated in time and the outputs of many receptor-enzyme "units" are added to produce the intracellular signal. Moreover, there are other sources of stochastic fluctuations within the cell and these may be equally important; to date the analysis has not been done for any signal transduction pathway. Stochastic effects are discussed by several authors (DeLisi & Marchetti, 1982; Tranquillo & Lauffenburger, 1987; Tranquillo & Alt, 1994) and we refer the interested reader to these sources.

An outline of the remainder of the paper is as follows. In Section 2 we discuss the governing equations for the system, using the model described in Tang & Othmer (1994, 1995) for the intracellular dynamics. In Section 3 we present numerical results for the case in which the intracellular dynamics are neglected and the flux at the boundary of one cell is a specified function of time. This allows us to investigate the interaction of extracellular factors with a fairly simple computation, the results of which shed light on the early chemotactic signal. In Section 4 we present numerical results for the full problem with both the extracellular equations and the intracellular dynamics which indicate the range of behavior that is possible. Again in these simulations the flux at one cell boundary is specified and the other cell responds to the imposed signal. In Section 5 we summarize and discuss the results.

2. The Mathematical Model

Our goal in this paper is to determine the spatio-temporal profile of cAMP seen by a cell when a neighboring cell signals, and to evaluate various mechanisms for orientation of the cell. In this section we develop the mathematical model which will be analysed in the following sections. The cells are assumed to be cylindrical in shape, having radius $r_0 = 5.5$ microns and height $h = 2$ microns. Thus the cells appear as disks on the plane when viewed from above, as shown in Fig. 1. The concentrations are assumed to be uniform in the vertical direction, and diffusion and degradation of cAMP occurs both within each cell and in the region exterior to the cells. Signal transduction and cAMP production occur at the boundary of each cell, and secretion occurs across that boundary.

2.1. THE MODEL FOR SIGNAL TRANSDUCTION AND CAMP PRODUCTION IN THE RELAY RESPONSE

Our model is based on the signal transduction and cAMP production scheme developed in Tang & Othmer (1994) and Tang & Othmer (1995). This model postulates two channels, an excitable one and an inhibitory one. Each utilizes G proteins, which are heterotrimeric proteins comprising α, β, and γ subunits. When the protein is activated the α subunit decouples from the $\beta\gamma$ complex, which forms a tightly coupled pair, to form two components. In the excitable pathway cAMP (denoted H) binds to the cell surface receptors cAR1 (denoted R_s) which detect extracellular cAMP, and the complex HR_s catalyses the activation of the α subunit G_s' of the stimulatory G protein G_s. This in turn binds with

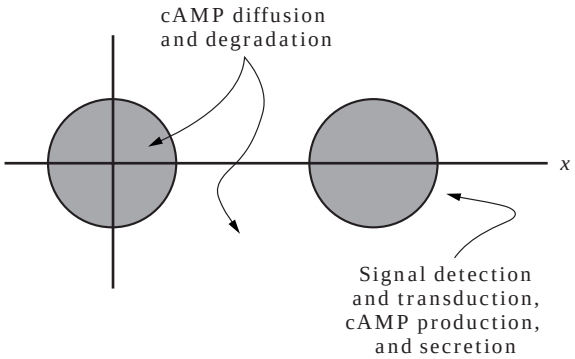

FIG. 1. The geometric arrangement of the two cells and the processes that are incorporated in the model.

the inactive form of adenylyl cyclase (AC), an enzyme which catalyses the production of cAMP, and produces the activated form $G_s'AC$. A GTP-ase activity intrinsic to the α subunit of the G protein terminates the activation. In the inhibitory pathway an inhibitory G protein subunit G_i' is produced by analogous steps. However, the symmetry between the pathways is broken at this point, because G_i' binds with HR_s, and in this bound form HR_s cannot activate G_s.

It was shown in Tang & Othmer (1995) that the system of equations describing the intracellular dynamics could be reduced to four equations. The model incorporates a basal activity of adenylate cyclase activity, and hence a constant background production of cAMP, as well as a secretion rate that depends on the level of cAMP. A low level of secretion is associated with the basal cAMP level, and a higher secretion rate occurs at cAMP levels characteristic of the relay response. The results of the model are compared with results from perfusion and suspension experiments done by Gerisch & Wick (1975), Devreotes & Steck (1979) and Tomchik & Devreotes (1981), and it is shown that the model provides a good input–output description of the response of cells to the stimulus protocols used in experiments.

2.1.1. *The extracellular reaction network and governing equations*

Three major processes occur in the extracellular medium: (i) cAMP secretion; (ii) cAMP degradation by either external phosphodiesterase (ePDE) or mPDE; and (iii) cAMP diffusion. The secretion and the degradation of cAMP by mPDE both occur at the cell membrane and lead to "boundary" conditions that couple the intra- and extracellular dynamics. Degradation of cAMP by ePDE occurs throughout the extracellular space. Thus the extracellular reactions can be grouped into two types: reactions which occur on the boundary of the cell and reactions that are valid in the extracellular medium. These reactions are as follows:

(i) reactions occurring on the boundary of each cell

$$cAMP_i \overset{dsr}{\rightarrow} cAMP_o$$

$$cAMP_o + \text{mPDE} \underset{l_{-6}}{\overset{l_6}{\rightleftarrows}} cAMP_o - \text{mPDE}$$

$$cAMP_o - \text{mPDE} \overset{l_7}{\rightarrow} \text{AMP} \qquad (1)$$

(ii) reactions occurring in the extracellular medium

$$cAMP_o + \text{ePDE} \underset{l_{-8}}{\overset{l_8}{\rightleftarrows}} cAMP_o - \text{ePDE}$$

$$cAMP_o - \text{ePDE} \overset{l_9}{\rightarrow} \text{AMP}. \qquad (2)$$

Here the subscripts i and o denotes intracellular and extracellular cAMP, respectively. AMP denotes adenosine monophosphate and *dsr* denotes the secretion rate function. The various constants are defined explicitly in Tang & Othmer (1994, 1995), where further details about the kinetic scheme can be found. The definitions of the symbols for the main species used here are given in Table 1.

The evolution equations for the extracellular species incorporate these reactions, as well as diffusion of cAMP. For simplicity we assume that ePDE is non-zero in a cylinder centered between the cells having radius 55 microns, and is zero elsewhere. In this disk ePDE is taken to be constant and we ignore diffusion of ePDE and its complex with cAMP. In reality, ePDE exists throughout the exterior region and its concentration decreases with distance from the cells, which secrete it, but the effect of ePDE is small compared with that of mPDE. The above reactions give the following two sets of

TABLE 1
The variables for the extracellular reactions

Species	Dimensional form	Dimensionless form
$[cAMP_i]$	y_{12}	$w_4 = \frac{y_{12}}{[\text{iPDE}]_T}$
$[cAMP_o]$	y_{14}	$w_5 = \frac{y_{14}}{[\text{iPDE}]_T}$
[mPDE-cAMP]	y_{15}	(a)
$[\text{ePDE-cAMP}_o]$	y_{16}	(a)
[mPDE]	z_8	(b)
[ePDE]	z_9	(b)

(a) Removed by singular perturbation.
(b) Removed by use of a conservation condition.

equations, which hold at any point in the extracellular medium.

$$\frac{\partial y_{14}}{\partial t} = D\bar{\nabla}^2 y_{14} + l_{-8} y_{16} - \frac{NV_c}{V_e} l_8 y_{14} z_9$$

$$\frac{\mathrm{d}y_{16}}{\mathrm{d}t} = -(l_{-8} + l_9) y_{16} + \frac{NV_c}{V_e} l_8 y_{14} z_9. \qquad (3)$$

Here $\bar{\nabla}^2$ is the dimensional Laplace operator in $\mathbf{R}^2$, D is the diffusion coefficient, V_e is the volume in which ePDE is present, V_c is the volume of a cell and N is the number of cells ($N = 2$).

The second set of equations, which applies on the boundary of each cell, is

$$-A_c D \frac{\partial y_{14}}{\partial \mathbf{n}_\mathbf{o}^i} = V_c dsr(y_{12}^i) + A_c l_{-6} y_{15}^i - A_c l_6 y_{14} z_8^i$$

$$\frac{\mathrm{d}y_{15}^i}{\mathrm{d}t} = -(l_{-6} + l_7) y_{15}^i + l_6 y_{14} z_8^i. \qquad (4)$$

Here the superscript i denotes the cell, $\mathbf{n}_\mathbf{o}^i$ is the outward normal direction for the i-th cell and $A_c = 2\pi r_0 h$ is the lateral area of a cell.

The conservation equations are

$$y_{15}^i + z_8^i = [\mathrm{mPDE}]_T^i$$

$$y_{16} + \frac{NV_c}{V_e} z_9 = \frac{NV_c}{V_e} [\mathrm{ePDE}]_T. \qquad (5)$$

Following the singular perturbation techniques used in Tang & Othmer (1995) and using the same non-dimensional variables, one obtains the following form for the equations:

$$\frac{\partial w_5}{\partial \tau} = \overbrace{D_1 \nabla^2 w_5}^{\text{diffusion of cAMP}} - \overbrace{\hat{\gamma}_9 \frac{w_5}{w_5 + \gamma_8}}^{\text{degradation due to ePDE}} \qquad (6)$$

where $D_1 = D/(k_5 r_0^2)$, $\hat{\gamma}_9 = \gamma_9 NV_c/V_e$, ∇^2 is the non-dimensional Laplace operator, and $\tau = t/k_5$.

The boundary condition at the exterior surface of each cell is

$$\overbrace{-D_1 \frac{\partial w_5}{\partial \hat{\mathbf{n}}_\mathbf{o}^i}}^{\text{outward flux of cAMP}} = \overbrace{-\gamma_7 \frac{w_5}{w_5 + \gamma_6}}^{\text{degradation due to mPDE}} \overbrace{+\frac{V_c}{A_c r_0} sr(w_4^i)}^{\text{secretion}} \qquad (7)$$

where $\hat{\mathbf{n}}_\mathbf{o}^i = \mathbf{n}_\mathbf{o}^i / r_0$ and $\gamma_7 = \ell_7 [\mathrm{mPDE}]_T / (k_5 [\mathrm{iPDE}]_T r_0)$. The function $sr(x)$ is the dimensionless secretion rate and is given by

$$sr(x) = \begin{cases} sr_1 x & \text{if } x \leqslant sw \\ sr_2(x - sw) + sr_1 sw & \text{if } x > sw \end{cases}. \qquad (8)$$

Equations (6) and (7) constitute the extracellular component of the model which is used in all of the numerical simulations. Next we describe the intracellular dynamics.

2.1.2. *Intracellular cAMP dynamics*

Transduction of an external cAMP signal into an intracellular signal is via proteins that are closely associated with the cell membrane. Consequently, in modeling the intracellular dynamics we assume that all processes except the degradation of cAMP by iPDE occur on the boundary, and we allow the cAMP to diffuse in the interior of the cell. In Tang & Othmer (1994, 1995) intracellular quantities are expressed relative to the area of the cell, and thus only the equations for cAMP_i and $\mathrm{iPDE\text{-}cAMP}_i$ have to be changed. The equations for these quantities become

$$\frac{\partial y_{12}^i}{\partial t} = D\bar{\nabla}^2 y_{12}^i + l_{-3} y_{13}^i - l_3 y_{12}^i z_7^i$$

$$\frac{\mathrm{d}y_{13}^i}{\mathrm{d}t} = -(l_{-3} + l_4) y_{13}^i + l_3 y_{12}^i z_7^i \qquad (9)$$

TABLE 2

The relationship between dimensional and dimensionless variables for the intracellular reactions

Species	Dimensional form	Dimensionless form
$[\mathrm{G}_s'\mathrm{AC}]$	y_4	$w_1 = \frac{y_4}{[\mathrm{UC}]_T}$
$[\mathrm{G}_i']$	y_8	$w_2 = \frac{y_8}{[\mathrm{G}_i]_T}$
$[\mathrm{HR}_s\mathrm{G}_i']$	y_9	$w_3 = \frac{y_9}{[\mathrm{R}_s]_T}$
$[\mathrm{G}_s'\mathrm{AC\text{-}ATP}]$	y_{11}	(a)
$[\mathrm{cAMP}_i]$	y_{12}	$w_4 = \frac{y_{12}}{[\mathrm{iPDE}]_T}$
$[\mathrm{iPDE\text{-}cAMP}_i]$	y_{13}	(a)
$[\mathrm{HR}_s]$	y_1	$u_1 = \frac{y_1}{[\mathrm{R}]_s]_T}$
$[\mathrm{G}_s']$	y_3	$u_2 = \frac{y_3}{[\mathrm{G}_s]_T}$
$[\mathrm{HR}_i]$	y_6	$u_4 = \frac{y_6}{[\mathrm{R}_i]_T}$
[UC]	z_3	(b)
[iPDE]	z_7	(b)

(a) Removed by singular perturbation.
(b) Removed by use of a conservation condition.

TABLE 3

The values of the dimensionless parameters. These are found by using the same base parameters as were used in Tang & Othmer (1995). *Because most of the conserved quantities used by Tang & Othmer are converted to concentrations the parameters* γ_4, β_4, γ_2, γ_7 *and* γ_9 *all have an additional factor of either the volume ratio* (*volume used by Tang and Othmer over volume assumed here*) *or area ratio* (*defined similarly*)

$\alpha_0 = 312.0$	$\beta_0 = 61.0$	$\gamma_1 = 323.2$	$\gamma_6 = 0.29$ or 11.6	$D_1 = 13.2$
$\alpha_1 = 0.8$	$\beta_1 = 16.0$	$\gamma_2 = 0.32$	$\gamma_7 = 67.3$	$sr_1 = 0.02$
$\alpha_2 = 2.67$	$\beta_2 = 0.48$	$\gamma_3 = 57.7$	$\Gamma_7 = 1.09$	$sr_2 = 0.65$
$\alpha_3 = 1.0$	$\beta_3 = 1.0$	$\gamma_4 = 350.0$	$L_7 = 0.09$	$sw = 0.5$
$\alpha_4 = 147.0$	$\beta_4 = 11.0 \times 10^4$	$\gamma_5 = 0.15$	$\gamma_8 = 750.0$	
	$\beta_5 = 0.4$	$\Gamma_5 = 1.2$	$\gamma_9 = 0.0$ or 2416.8	
	$\beta_6 = 204.0$			

for the interior of each cell where the superscript i denotes the cell as before. The boundary condition on the interior side of the boundary is that the inward normal component of the flux is equal to the production of cAMP at the boundary minus the secretion. Thus

$$-\mathbf{n_i}\cdot(A_c D\bar{\nabla} y_{12}^i) = -A_c D\frac{\partial y_{12}^i}{\partial \mathbf{n_i^i}} = A_c l_2 y_{11}^i + A_c l_5 z_3^i - V_c dsr(y_{12}^i). \quad (10)$$

where $\mathbf{n}_i$ is now the *inward* normal to the boundary. The symbols for the dimensional and non-dimensional form of the intracellular species are given in Table 2.

After converting the variables to dimensionless form and performing the singular perturbation these equations become

$$\frac{\partial w_4^i}{\partial \tau} = \overbrace{D_1\nabla^2 w_4^i}^{\text{diffusion of cAMP}} - \overbrace{\gamma_4\frac{w_4^i}{w_4^i+\gamma_3}}^{\text{degradation due to iPDE}} \quad (11)$$

in the interior of each cell, and the boundary conditions are

$$\overbrace{-D_1\frac{\partial w_4^i}{\partial \hat{\mathbf{n}}_\mathbf{i}^i}}^{\text{inward flux of cAMP}} = \overbrace{\gamma_1\gamma_2 w_1^i}^{\text{stimulated production}} + \overbrace{\Gamma_5(1-\Gamma_7 w_1^i)}^{\text{basal production}} - \overbrace{\frac{V_c}{A_c r_0} sr(w_4^i)}^{\text{secretion}} \quad (12)$$

where $\Gamma_7 = 1 - L_7$, $L_7 = \ell_1/(\ell_{-1} + \ell_2)$, $\gamma_2 = \ell_2[\mathrm{UC}]_T/(\ell_{-1} + \ell_2)[\mathrm{iPDE}]_T r_0$, $\hat{\mathbf{n}}_\mathbf{i}^i = \mathbf{n}_\mathbf{i}^i/r_0$, $\Gamma_5 = \gamma_5/(1 + L_5)$, $L_5 = (\ell_{-5} + \ell_5^*)(\ell_5[\mathrm{ATP}])$ and $\gamma_5 = \ell_5^*[\mathrm{UC}]_T/(k_5[\mathrm{iPDE}]_T r_0)$. The parameter values used are given in Table 3.

These are the same values as were used in Tang & Othmer (1995) with the exception of K_{mPDE} (and the cell geometry already mentioned), which is allowed to vary, and γ_5. The variation of K_{mPDE} is reflected in γ_6. Because a different cell geometry is used here, γ_5 has been scaled such that the cAMP concentration in the unstimulated cell is maintained at about 0.8 μM, which compares well with biologically-measured values. The non-dimensionalization is similar to that in Tang & Othmer (1995).

The membrane-bound components evolve according to the equations

$$\frac{\mathrm{d}w_1^i}{\mathrm{d}\tau} = \alpha_4 u_2^i - w_1^i - \alpha_4 u_2^i w_1^i$$

$$\frac{\mathrm{d}w_2^i}{\mathrm{d}\tau} = \beta_2\beta_3 c_2 u_4^i - \beta_5 w_2^i + \beta_6 c_3 w_3^i - c_3\beta_4 u_1^i w_2 - \beta_2\beta_3 c_2 u_4^i(w_2^i + c_3 w_3^i)$$

$$\frac{\mathrm{d}w_3^i}{\mathrm{d}\tau} = -(\beta_5 + \beta_6)w_3^i + \beta_4 u_1^i w_2^i$$

$$u_1^i = \frac{\alpha_0 w_5^i + (\beta_5 - \alpha_0 w_5^i)w_3^i}{\alpha_1 + \alpha_0 w_5^i + \beta_4 w_2^i}$$

$$u_2^i = \frac{\alpha_2\alpha_3 c_1 u_1^i(1 - w_1^i)}{1 + \alpha_4 + \alpha_2\alpha_3 c_1 u_1^i - \alpha_4 w_1^i}$$

$$u_4^i = \frac{\beta_0 w_5^i}{\beta_1 + \beta_0 w_5^i}. \quad (13)$$

The first equation in (13) describes the evolution of the activated adenylate cyclase (w_1). Its production is stimulated by the activated α subunit of the G protein in the stimulatory pathway (u_2) which in turn is created by the

bound receptor (u_1). The second equation describes the evolution of the amount of the activated α subunit of the G protein in the inhibitory pathway (w_2). This is activated by a bound inhibitory receptor (u_4) and shuts down the stimulatory pathway by binding with the bound receptor (u_1) to form w_3.

This completes the development of the governing equations in their full generality. We will use eqns (11), (12) and (13) in Section 4, but we first study the exterior eqns (6) and (7) in the following section.

2.2. REMARKS ON THE NUMERICAL PROCEDURES

In the model cAMP diffusion occurs both within the cells and in the extracellular medium. In the extracellular medium the spatial scale of interest for signal transmission varies from at least ~ 5 microns to over 60 microns, depending on the separation between the cells. However in the interior of a cell the signal is transmitted on scales ranging from a fraction of a micron up to 11 microns (the diameter of the cell). A characteristic time for diffusion over a distance x is given by $\tau = x^2/4D$, where D is the diffusion coefficient. We use $D = 2.5 \times 10^{-6}\,\mathrm{cm}^2/\mathrm{s}$ (Tang & Othmer, 1995), so $\tau \sim \mathcal{O}(0.1)$ seconds for $x = 10$ microns, and of order 3.6 s for $x = 60$ microns. The large disparity between the time-scales for the interior and exterior problems means that the governing equations have widely-different time (and space) scales, and this makes the equations difficult to solve (''stiff'' in the terminology of numerical analysis). Furthermore, the exterior cAMP concentration varies most rapidly along the centerline between cells and near the periphery of the cells and less rapidly elsewhere.

In order to deal with these problems we have developed a special numerical algorithm. We scale the equations as given above, but the interior equations are discretized using a finer space and time mesh than are the exterior equations. To allow for the disparity in time steps we use a split time step method for dealing with the interior and exterior equations. Furthermore we use a non-uniform spatial discretization for the exterior equations, with finer resolution near the surfaces of the cells and in the region between the cells than elsewhere. This leads to a computationally robust algorithm that is still not prohibitive in terms of the computational time required. The details of the algorithm and its implementation are given in the Appendix and in Dallon (1996).

3. The Spatio-temporal Signal in the Absence of Signaling by the Receiver

3.1. THE EXTERIOR EQUATIONS

Relay-competent cells must quickly decide on the direction in which to move after receiving a signal, since they will relay the signal and thus *seemingly* obliviate any directional information in the extracellular cAMP distribution. It is known that the cGMP pathway, which is important in controlling the cell motion (Van Haastert & Van der Heijden, 1983; Kuwayama *et al*., 1993; Ross & Newell, 1981), responds on a faster time-scale than does the cAMP pathway, and that the intracellular cGMP peaks about 10 seconds after stimulation (Valkema & Haastert, 1994). In order to gain some insight into the mechanism by which the cell determines a direction to move, we first analyse the interactions between the various extracellular processes in the early stages of signaling by considering a problem in which the intracellular dynamics are turned off. In this section one cell functions as the signaler by releasing cAMP with a specified time course, and the other cell serves as the receiver but does not release cAMP. This is a realistic model for the early stages since a single cell can be a pacemaker (DeYoung *et al*., 1988), and each cell relays the signal. In addition, there are mutant cells which cannot relay cAMP but do orient and chemotact (Glazer & Newell, 1981). A careful study to determine if they orient as effectively as normal relaying Dd cells has not been performed. Nevertheless, they are able to orient with the characteristics of the signal we model here. To determine the cAMP concentration in the two-dimensional region exterior to the cells, we must solve the reaction-diffusion equation

$$\frac{\partial w_5}{\partial \tau} = D_1 \nabla^2 w_5 - \hat{\gamma}_9 \frac{w_5}{w_5 + \gamma_8} \tag{14}$$

exterior to the cells, with boundary conditions

$$-D_1\hat{\mathbf{n}}_o^1\cdot\nabla w_5 = -\gamma_7\frac{w_5}{w_5+\gamma_6} \tag{15}$$

on the boundary of the receiver and

$$-D_1\hat{\mathbf{n}}_o^2\cdot\nabla w_5 = \frac{V_c}{k_5[\mathrm{iPDE}]_T A_c r_0}KF(t) - H(t-2)\left(\gamma_7\frac{w_5}{w_5+\gamma_6}\right) \tag{16}$$

on the boundary of the signaling cell. Here $\hat{\mathbf{n}}_o^i$ is the outward normal to the cell boundary, as before, and $K^{-1} = V_c \times$ Avagadro's number. The function $F(t)$ takes into account not only the release of cAMP by the signaling cell, but also enzymatic degradation by mPDE on the cell surface [cf. eqn. (7)]. It is taken to be a piecewise linear function defined by

$$F(t) = \begin{cases} F_m t & 0 \leqslant t < 1 \\ F_m(2-t) & 1 \leqslant t \leqslant 2 \\ 0 & \text{otherwise} \end{cases} \tag{17}$$

where t is in minutes and F_m is set at 2×10^7 molecules per cell per minute[2] (Roos *et al*., 1975; Gerisch & Wick, 1975). We turn the signaling on for 2 minutes because this is the nominal signaling period in response to a step change in extracellular cAMP. H is the Heaviside function, which is defined as

$$H(t) = \begin{cases} 0 & t < 0 \\ 1 & t \geqslant 0 \end{cases}. \tag{18}$$

Because F takes into account the degradation by mPDE, the effect of mPDE must be turned on separately when the signal is terminated at $t = 2$ min, which accounts for the term involving $H(t)$.

3.2. NUMERICAL RESULTS

Attenuation of the cAMP signal transmitted from a signaling cell to a receiver is due to both diffusive spread of the signal and hydrolysis due to the phosphodiesterase present. The interplay of these factors is complex, particularly when the distance between signaler and receiver is also varied. This was first shown in a model with no intracellular dynamics developed in Pate *et al*. (1988). Here we present a series of simulations to indicate how each factor affects the global cAMP signal. We first consider diffusive signaling between two cells in the absence of any ePDE but in the presence of mPDE. The value of the effective Michaelis constant for mPDE, which we denote K_{mPDE}, has a reported range of 0.5 to 20.0 μM (Malchow *et al*., 1975; Green & Newell, 1975). At the lowest affinity reported ($K_{mPDE} = 20.0\ \mu$M) $\gamma_6 = 11.6$, while at the highest reported affinity ($K_{mPDE} = 0.5\ \mu$M) $\gamma_6 = 0.29$. The use of these values will produce chemical profiles which bracket the true profiles seen by a cell. In addition, the low-affinity results should closely approximate the profiles when mPDE is completely blocked. At the end of this section we remark on the effect of including ePDE.

In the first set of simulations we set $K_{mPDE} = 20.0\ \mu$M and, because there is no ePDE, $\gamma_9 = 0$. The center-to-center spacing between the signaling and receiving cells is set at either 30 microns approximately half of the maximum separation at which aggregation long-range signaling occurs (Gingle, 1976; Konijn & Raper, 1961), or 5 microns. Figure 2 displays the concentration profile 12 seconds after the start of the 2 minute secretion period. The time at which to display the profiles was chosen for two reasons. Firstly, cells can certainly orient within 20 seconds after receiving a stimulus (Futrelle *et al*., 1982) (and faster in some reports), which indicates that the choice of direction is made in this time frame. Secondly, the cGMP signal, which is involved in chemotaxis, peaks about 10–15 seconds after stimulation. Although the 2 minute duration of the secretion function is biologically relevant, changing it in the simulations does not affect the qualitative behavior in any significant way. Thus one can compare our results with the work of Soll *et al*. (1993), where cells are exposed to waves of duration 7 minutes and orient within the first 8% of the wave duration.

In Fig. 2 the solid curve gives the concentration profile along the half-line extending from the center of the signaling cell through the center of the receiving cell, while the dashed line shows the profile along the antipodal direction. Although the cAMP concentration is ultimately

monotonically decreasing in both directions, there are distinct differences locally due to the presence of the receiving cell. In panels (a) and (c) one sees that the local cAMP gradient is decreased in magnitude near the receiver as compared with the opposite direction. Due to the "diffusion shadow" created by the receiving cell, both the difference between the front and rear concentrations and the front/rear ratio of cAMP concentrations increases over that of the unperturbed field in the same spatial region. (Front will always refer to that point on the receiving cell closest to the signaling cell, rear to the point furthest away.) Thus the mere presence of the receiving cell amplifies any chemotactic signal based on a front-to-back concentration difference when compared with the field generated by the signaling cell alone. This effect is accentuated as the intracellular distance decreases, as can be seen by comparing panels (a) and (c). Since the cell separation does not affect any of the results of this section qualitatively, the separation will hereafter be set at 30 microns unless stated otherwise.

The second aspect concerns the effect of mPDE on the profiles, and to understand this we reduce the effective Michaelis constant to $K_{mPDE} = 0.5\ \mu$M, which makes $\gamma_6 = 0.29$. Panels (b) and (d) of Fig. 2 show the resulting concentration profiles. In comparing panels (a) and (c) with panels (b) and (d), we see that the chemoattractant levels are everywhere lowered in the latter due to increased enzymatic degradation, and there is a distinctive sharpening of the cAMP spatial gradient between the signaling and receiving cell (solid line) as was suggested previously on the basis of a less detailed model (Nanjundiah & Malchow, 1976). In fact the concentration at the receiving cell has been decreased by more than a factor of 2 as

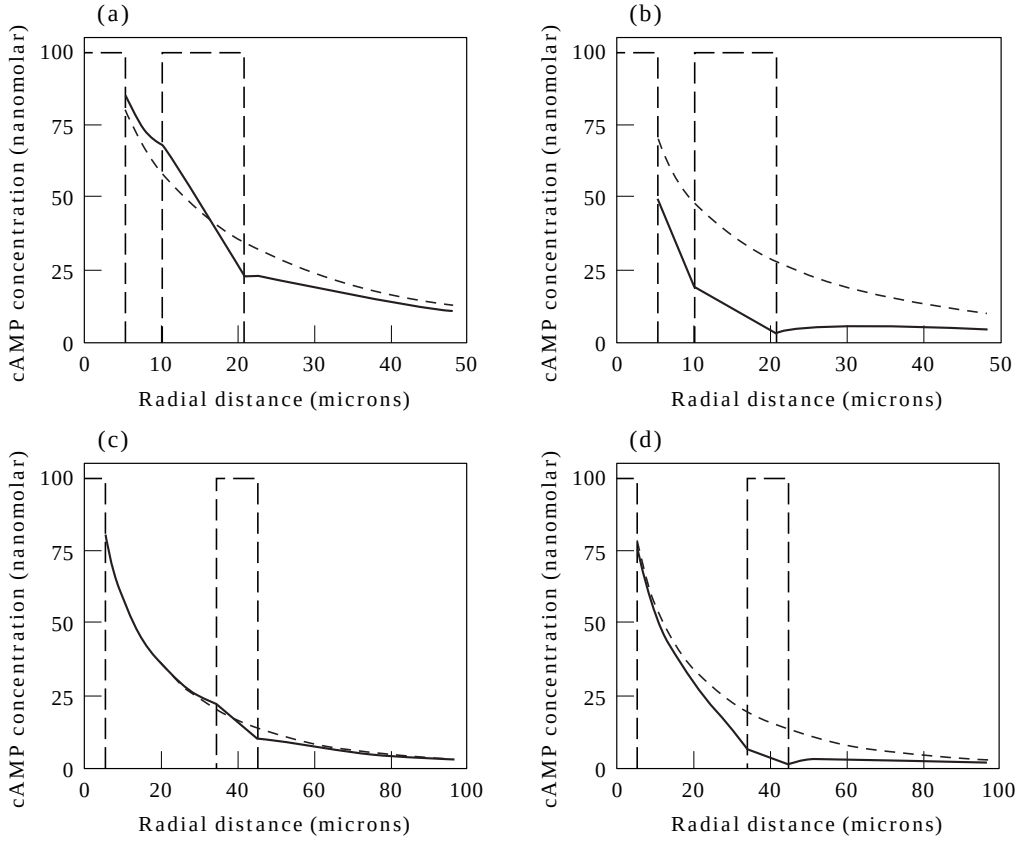

FIG. 2. The concentration profile of cAMP when one cell is signaling and the receiver is inactive. The large dashed rectangles represent the cells; the signaling cell is on the left and the receiver is on the right. In panels (a) and (b) the cell separation is 5 microns; in (c) and (d) it is 30 microns. In (a) and (c) $\gamma_6 = 11.6$, while in (b) and (d) $\gamma_6 = 0.29$. All the profiles shown are at 12 seconds after the onset of signaling. The solid line is the cAMP concentration along the radius passing through the center of the receiver, and the dashed line is the cAMP concentration in the antipodal direction.

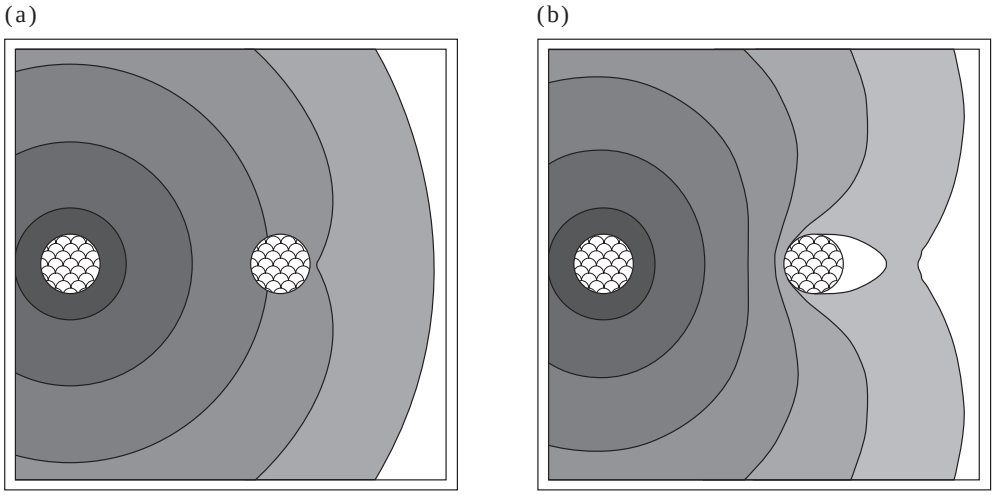

FIG. 3. A contour plot of the cAMP concentration in an 85 micron square region 12 seconds after the onset of signaling. The cells are 30 microns apart, the signaling cell is the circle on the left and the receiving cell is the circle on the right. In panel (a) $K_{mPDE} = 20.0\ \mu$M and in panel (b) $K_{mPDE} = 0.5\ \mu$M. The contours in (a) from highest (dark represents high concentration) to lowest are $10^{1.75}$ nM, $10^{1.50}$ nM, $10^{1.25}$ nM, 10 nM, $10^{0.75}$ nM and in (b) they are the same with one additional contour of $10^{0.5}$ nM.

compared with either the concentration in the antipodal direction or to the concentration at the receiving cell in the presence of lower mPDE activity [panels (a) and (c)]. Thus the presence of mPDE can have a major effect on the cAMP profiles, both at a fixed time, and as we shall see shortly, on the temporal profiles.

The effect of mPDE may extend a substantial distance from the receiving cell, as is shown by the level curves in Fig. 3. One can see that the concentration level lines are nearly circular when the affinity of mPDE is low [panel (a)], but in the high-affinity case the level sets are severely distorted [panel (b)]. In fact, in the latter case the receiving cell is located at a local minimum of the cAMP concentration: the concentration increases significantly in the direction normal to the boundary of the receiving cell at all points of the boundary.

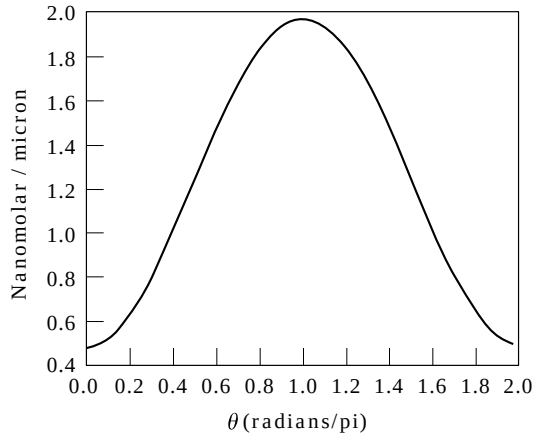

FIG. 4. The derivative of cAMP concentration with respect to the outward normal at the surface of the receiving cell for $K_{mPDE} = 0.5\ \mu$M. The signaling cell is in the direction $\theta = 1.0$.

This is further emphasized by the graph in Fig. 4, which shows that the spatial gradient in cAMP concentration normal to the receiving cell surface is everywhere positive, with a maximum value in the direction of the signaling cell. This is easily understood given the presence of mPDE on the cell membrane, but had been overlooked prior to the work of Pate *et al*. (1988). It should be noted that the maximum gradient seen by the receiver, which is $\sim 2 \times 10^3$ nM mm^{-1}, is far larger than either the static gradients of ~ 10 nM mm^{-1} used experimentally (Fisher *et al*., 1989) or the average gradient of ~ 100 nM mm^{-1} in an aggregation wave (Tang & Othmer, 1995).

To better characterize the cAMP signal at the receiving cell, we show the front (solid line) and rear (dashed line) cAMP concentrations at the receiving cell as a function of time in Fig. 5, and the front/rear cAMP ratio as a function of time in Fig. 6.

The time rates of change of cAMP concentration at the front (solid line) and rear (dashed

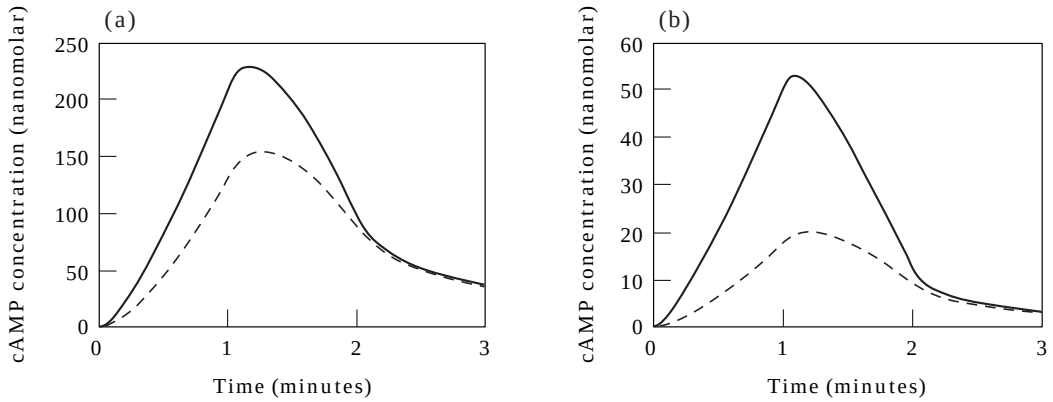

FIG. 5. The concentration of cAMP as a function of time for the same conditions as in Fig. 3. The solid (dashed) line corresponds to the concentration at the front (back) of the cell. Note the difference in the scales for the cAMP concentration in the two panels.

line) of the receiving cell are shown in Fig. 7 and the corresponding ratio is shown in Fig. 8.

The detailed information given in these figures on the spatio-temporal cAMP signal seen by a cell is significant for understanding what aspects of the signal could be used to determine the direction of movement. All of the characteristics of the solution shown in the figures have been suggested as candidates for determining the chemotactic response. However it is very unlikely that one of the above, namely the ratio of the rates of change at front and back, is used. One sees in Fig. 8 that this ratio is essentially constant during the early phase of signaling, and peaks *when both rates of change are negative*.

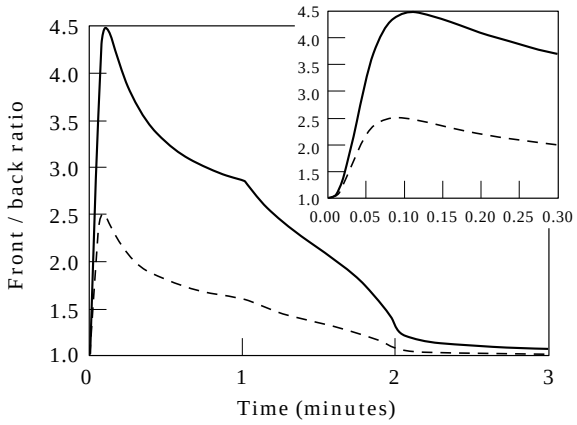

FIG. 6. The ratio of front and back cAMP concentrations at the receiving cell's surface for the time plots in Fig. 5. The solid line is the ratio for $K_{mPDE} = 0.5\ \mu$M and the dashed line is the ratio for $K_{mPDE} = 20.0\ \mu$M. The inset shows the short-time behavior of the ratios.

Moreover, as we will show in the following section, the peak occurs far too late to provide reliable information for orientation.

In the Introduction we described two other mechanisms that might plausibly be used, a spatial gradient sensing mechanism, in which the cell measures the concentration difference or the difference in the number of occupied receptors between front and back (Mato *et al*., 1975; Zigmond, 1978; McRobbie, 1986). and a "pseudo-spatial" mechanism in which cells extend pseudopods and convert the spatial gradient in attractant sensed into a temporal rate of change of attractant (Gerisch *et al*., 1975a). However, Figs 2, 3 and 4 show that in the presence of significant mPDE activity the cell sees an increase in the attractant in *every* direction. This result does not preclude the use of either mechanism, but the problem of choosing a direction in which to move becomes harder for the cell and thus orientation becomes less reliable. Using either of these mechanisms, the problem is not to choose between favorable and unfavorable directions, as would be the case in the presence of a monotonic concentration profile across the cell, but rather that of selecting the best direction when all are favorable. In the absence of significant mPDE activity [cf. Fig. 2(a)], the directional derivative of cAMP in the normal direction is small within a pseudopod length of the cell in all directions, and a cell has an equally difficult problem deciding on the direction of movement. This prediction could be tested experimentally by blocking both mPDE

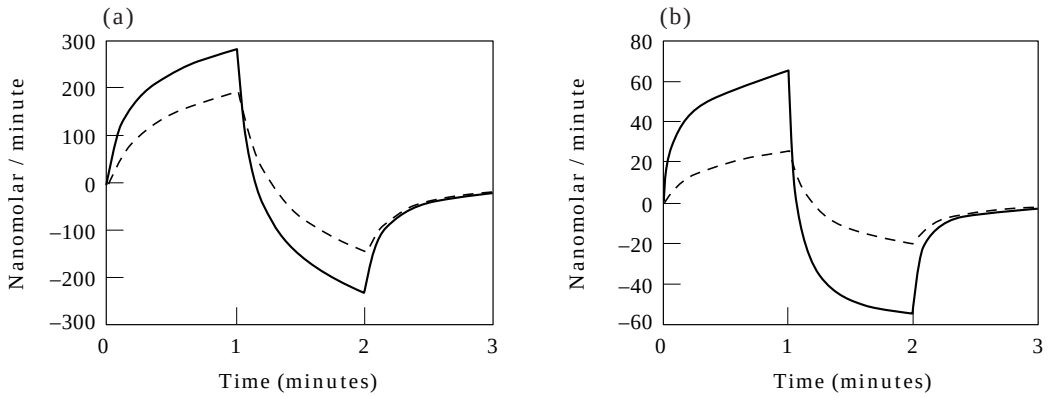

FIG. 7. The time rate of change at cAMP concentration at the surface of the receiving cell for the conditions in the previous two figures. The solid line indicates the front of the cell and the dashed line indicates the back of the cell.

and the secretion, and administering a cAMP stimulus using a micropipette.

Figure 5 shows the front (dashed line) and rear (solid line) cAMP concentrations as a function of time. Comparing part (a) and part (b) of Figs 2 and 5 it is evident that the increased affinity of the mPDE leads to a decrease in the absolute front-to-rear concentration difference across the receiving cell by a factor of two over that with a lower affinity mPDE. However, because the concentration decreases, the peak front-to-back ratio of cAMP increases by a factor of nearly two when compared with what exists for the low affinity mPDE (cf. Fig. 6). It is intuitively clear and will be shown explicitly later that this extracellular cAMP ratio is transduced into an intracellular cAMP gradient across the cell, and this can provide the directional information needed by a cell for orientation. Furthermore, the front-to-back ratio peaks early in the signaling period, which enables the cell to choose a direction for movement before it swamps the signal with the relay response. Use of this signal characteristic for orientation would also circumvent the difficulty associated with a gradient detection mechanism mentioned above, namely that the cAMP concentration near the cell is increasing outwardly in all directions. Thus, this ratio provides a better signal characteristic to use for initiating the chemotactic response than the local gradient at the surface (Gerisch *et al*., 1975b).

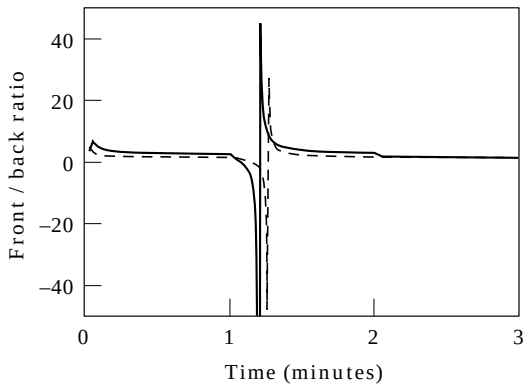

FIG. 8. Front-to-back ratio of the time rate of change for cAMP concentration. The solid line is the ratio with $\gamma_6 = 0.29$ and the dashed line is the ratio with $\gamma_6 = 11.6$.

An additional cAMP hydrolysing phosphodiesterase is secreted into the extracellular medium during the vegetative phase. An inhibitor of this enzyme is present during aggregation which raises the K_m of this enzyme from the micromolar to the millimolar range (Kressin *et al*., 1979). Addition of this enzyme to the previous simulation of signaling cells located 30 μm apart with the mPDE present results in virtually no modification of the cAMP environment near the receiving (or signaling) cell. Thus ePDE does not play an important role here since cAMP levels are low, a conclusion reached earlier by Nanjundiah & Malchow (1976). Of course ePDE affects the concentration levels somewhat and may be more important in waves, where it helps to prevent cAMP from rising to saturation levels (Darmon *et al*., 1978; Brachet *et al*., 1979).

4. The Effect of cAMP Production on the Extra- and Intracellular Signals

As we mentioned earlier, the extracellular cAMP differences seen by a cell are transduced

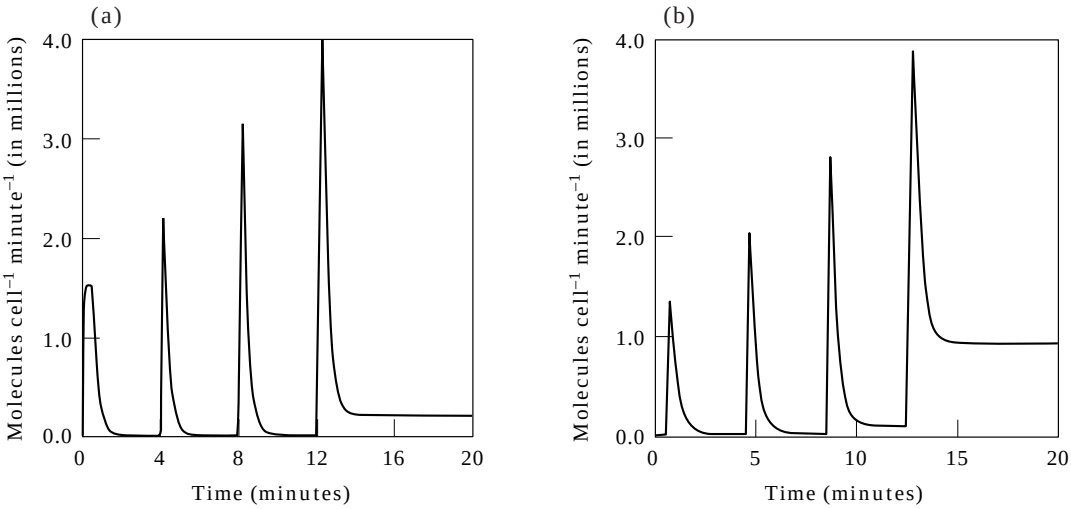

FIG. 9. The secretion response under clamped extracellular cAMP from the present model, in which AC is localized at the cell membrane (a) and simulated perfusion experiment using the Tang–Othmer model (b). The extracellular cAMP concentration is changed from 0 at $t = 0$ to 0.001 μM. Every 4 minutes thereafter it is increased by a factor of 10 until at $t = 12$ minutes the cAMP concentration is 1.0 μM. [Panel (b) is reproduced from Tang & Othmer (1995) with permission.]

into an intracellular gradient of cAMP or another species, such as cGMP, that is part of the cAMP signal transduction pathway. Such an intracellular gradient can be used to orient the cell if it can be set up sufficiently rapidly and maintained for a suitable period of time. However the spatio-temporal details of how it evolves can only be determined by incorporating the intracellular dynamics, and we do this for cAMP in this section. We solve the full system of equations described by eqns (6) and (11), with boundary conditions given by eqns (7), (12) and (13). As before we consider two cells on an infinite domain and assume that there is no ePDE present.

Since the underlying equations and numerical procedures are significantly more complicated than in the absence of intracellular dynamics, we first tested the computational procedure. To this end, the extracellular cAMP concentration was fixed at the boundary of the cell and the same four step stimulus used in perfusion experiments (Devreotes & Steck, 1979) was given. At $t = 0$ the extracellular cAMP concentration was set at 0.001 μM and held for 4 minutes, at $t = 4$ it was increased by a factor of 10 and held for 4 more minutes, and a similar increase was imposed at $t = 8$ and $t = 12$. In Fig. 9(a) we show the response for the four step stimulus, which should be compared with Fig. 9(b) from Tang & Othmer, (1995). The peak secretion rate and the duration of secretion are essentially the same as in the Tang–Othmer model, despite the fact that here AC is localized at the membrane, whereas in the Tang–Othmer model the interior of the cell is spatially homogeneous. This reflects the fact that the intracellular cAMP gradients are very small in the presence of a spatially-uniform and constant extracellular cAMP concentration. Moreover, adaptation at high stimulus levels is better here. The only significant difference between the two simulations is that the intracellular cAMP concentrations (not shown) are higher here because the different cell geometry of the cell used here implies that the concentrations have to be higher when the cell is stimulated in order to obtain the observed secretion rate per cell.

4.1. THE SIGNAL AT THE RECEIVER WHEN INTRACELLULAR CAMP PRODUCTION IS INCORPORATED

In the following series of tests only the receiving cell has active cAMP production, whereas the signaling cell has a prescribed function for the boundary condition, as described by (16) and (17). To facilitate comparison and to better understand the effect of relay on the ability of a cell to orient we use the same

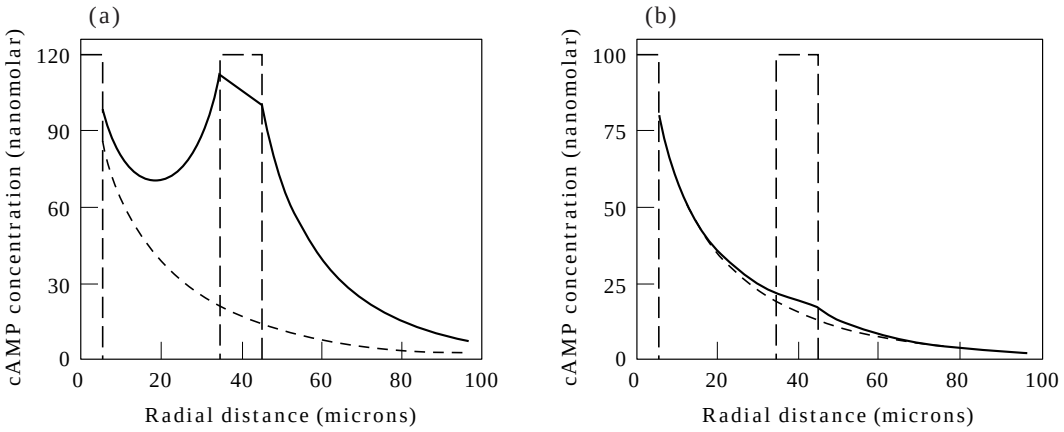

FIG. 10. The profile of cAMP concentration at $t = 12$ seconds when one cell signals and the receiver is active. In (a) $\gamma_6 = 11.6$ (low-affinity mPDE) and in (b) $\gamma_6 = 0.29$ (high-affinity mPDE) and in both panels the cell separation is 30 microns. The solid line is the cAMP concentration and the dashed line is the cAMP concentration in the antipodal direction. The signaling cell is on the left and the receiving cell is on the right.

cell spacings and mPDE levels here as were used in the previous section.

In Fig. 10 we plot the concentration profiles between the cells 12 seconds after the signaling was initiated.

In both panels the cAMP secretion rate is above the basal rate, i.e. the relay response has begun. The profiles shown, which are at a fixed instant in time, depend upon the initial state of the cell: a fully recovered cell will respond more quickly to a superthreshold signal than one that has been stimulated recently and is not fully recovered. However, the spatial profiles shown in the following figures are not qualitatively altered (provided that the cell has recovered enough to relay the signal), but the peaks caused by the relay response are shifted in time. As a result, if a cell determines its orientation after a fixed interval following stimulation, it may see a different spatial profile, depending on whether or not it is fully recovered. In particular, the spatial profile may be either as shown in Fig. 2(c) or as in Fig. 10(a) for low mPDE activity, and either as shown in Fig. 2(d) or as in Fig. 10(b) for high mPDE activity. A comparison of Figs 2(d) and 10(b) shows that in the presence of relay the cell only sees increasing concentrations in the direction of the signaling cell *at this time*, not in all directions, and in this case the "pseudo-spatial" mechanism might be effective. However this depends critically on the time at which a decision is made, for if one looks at the profile in the preceding case at a slightly later time the directional information is swamped. It should also be noted that the cells may not be able to aggregate when the mPDE activity is low, because the relay response quickly overwhelms the directional signal [cf. Fig. 10(a)]. This is qualitatively in agreement with what is found experimentally in mutants lacking mPDE (Brachet *et al.*, 1979), and in those experiments aggregation could be restored by placing the system over a large reservoir, which allowed cAMP to diffuse away more rapidly.

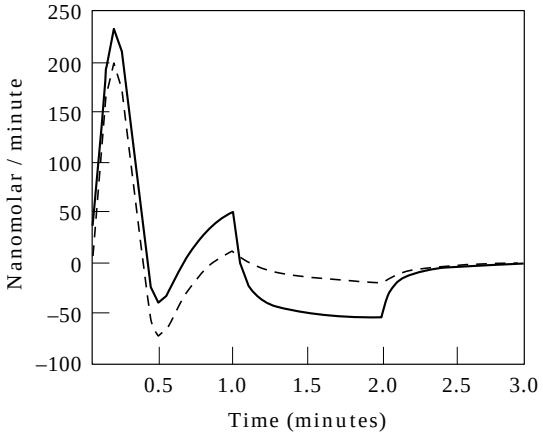

FIG. 11. The time rate of change of the extracellular cAMP concentration when the receiver is active. The solid line indicates the rate at the front of the cell and the dashed line indicates the rate at the back of the cell. In this simulation the cell separation is 30 microns and $\gamma_6 = 0.29$.

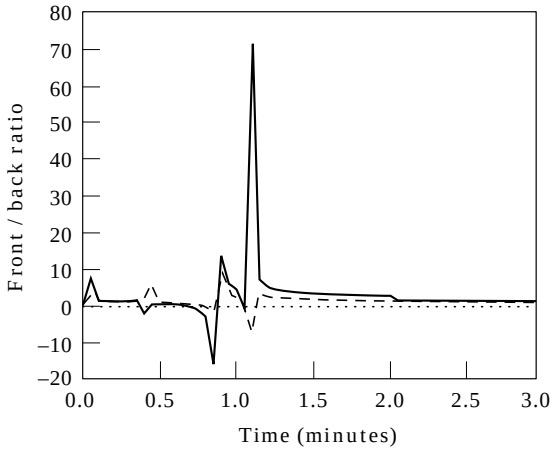

FIG. 12. Front-to-back ratio of the time rate of change for the extracellular cAMP concentration. The solid line represents the ratio for high-affinity mPDE, and the dashed line is the ratio for low-affinity mPDE.

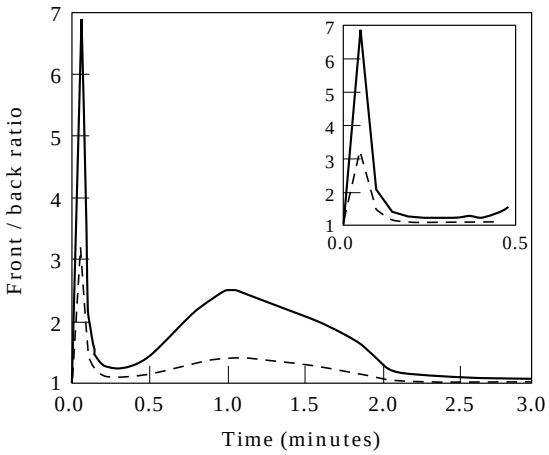

FIG. 14. Front-to-back ratio of extracellular cAMP concentration at the receiving cell's surface. The solid line is the ratio for $\gamma_6 = 0.29$ and the dashed line is the ratio for $\gamma_6 = 11.6$.

The time derivatives may change dramatically when the internal dynamics are added. In the absence of cAMP production the time derivative will indicate when the signal peaks, but that point conveys little information (cf. Fig. 7).

In the presence of cAMP production, the time derivatives at the front and back have a large peak at about 10 seconds, which is soon after the relay response begins (cf. Fig. 11). This characteristic of the signal could be used to initiate movement as follows. If there is an intracellular "motion controller" that adapts to constant extracellular cAMP signals, as both cAMP and cGMP do, then an effective rule for determining when to move [which is done separately from the choice of direction (Van Duijn & Van Haastert, 1992)] is simply to begin movement whenever this substance exceeds a threshold. Coincidentally, the temporal profile of actin polymerization in *D. mucorides* is very similar to the profile of the cAMP derivatives shown in Fig. 11 (cf. Fig. 1 in Newell, 1986). Depending on how rapidly this quantity adapts, it may or may not also determine how long to move. A movement rule based on above-threshold levels of a substance that adapts to extracellular cAMP levels was the most successful one of several explored in Dallon & Othmer (1997).

However, one also sees in Fig. 11 that the front-to-back difference of the time derivatives is probably not large enough to *orient* the cell.

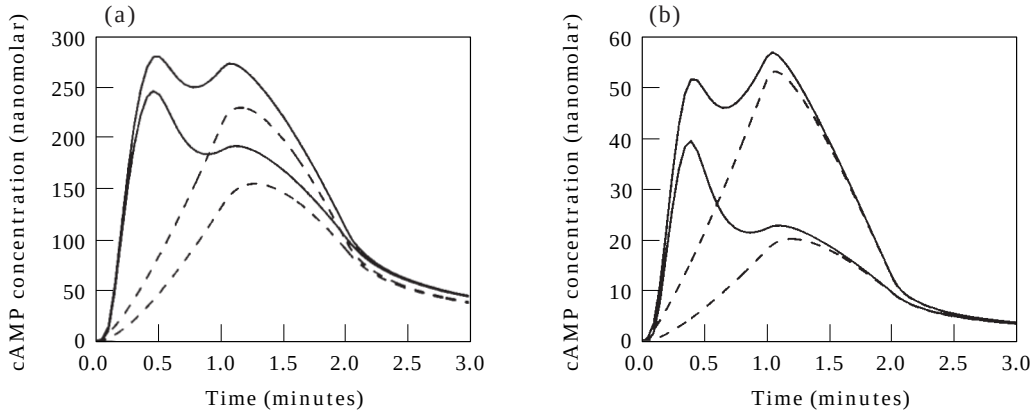

FIG. 13. Concentration of extracellular cAMP plotted in time. The upper solid (dashed) lines indicate the concentration at the front of the active (inactive) cell and the lower solid (dashed) lines are at the back of the active (inactive) cell. The dashed lines are the same as in Fig. 5. In (a) $\gamma_6 = 11.6$ (low affinity in mPDE) and in (b) $\gamma_6 = 0.29$ (high affinity in mPDE).

Figure 12 shows that there is some directional information in the ratio of the rates, but it is overshadowed by other less informative peaks that occur later. In fact, the major peak coincides time-wise with the peak in the absence of intracellular cAMP production (cf. Fig. 8). Thus the characteristic of the signal is a good candidate for initiating cell movement, but it seems doubtful it would be used to orient the cell.

Figure 13 shows that inclusion of the relay response also alters the time course of cAMP significantly, particularly in the initial phase signaling. In both panels *the first peak is due to the relay response of the receiving cell* and the second peak is due to the peak in the signal from the signaling cell. Since we have used a linearly increasing and decreasing signal with a half width of 1 minute, the relay signal dominates the concentration profile initially because the transduction pathway is fast when compared with this time and to the time-scale of the diffusion of cAMP.

The front-to-back ratio of the extracellular cAMP concentrations is shown in Fig. 14. A comparison of this figure with Fig. 6 shows that incorporating the relay response shortens the duration of the spike in this ratio. If this is used for orientation then the time a cell has to orient is reduced by the relay response, but the signal is not obliterated. In fact, for both values of γ_6 the peak is greater than when the cell is inactive. Furthermore, the front-to-back ratio is the signal characteristic that is the most strongly influenced by the cell separation: the closer the cell is to the signaler the greater is this ratio (results not shown). Thus the ratio has all the characteristics needed to serve for reliably orienting the cell, if it is properly transduced into an intracellular signal.

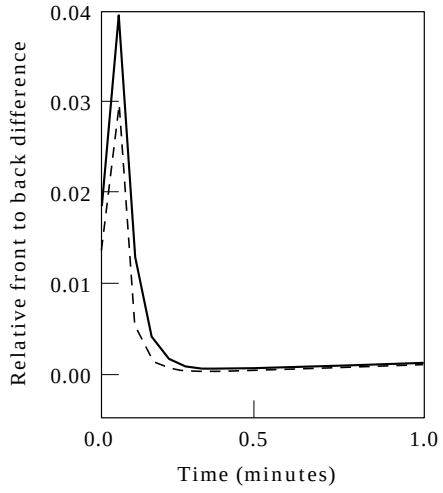

FIG. 15. The relative front to back difference of internal cAMP concentration (front-back/front) for the receiving cell. The solid line is the difference for $\gamma_6 = 0.29$ and the dashed line is the difference for $\gamma_6 = 11.6$.

To see what can be expected, consider the *internal* cAMP concentration at the front and back of the cell. As is seen in Fig. 15, the difference is small because intracellular cAMP is free to diffuse throughout the cell. Because the cAMP gradient is small, it is probably not used for orientation, and a much larger gradient of some other species could be established in several ways. Firstly, if signal transduction activates a membrane-bound factor, then the intracellular gradient of that factor can be made large simply by incorporating the appropriate amount of amplification into the pathway. Such a membrane-bound factor might, for instance, be a catalytic site for actin polymerization. Alternatively, even if the intracellular factor that determines orientation is a diffusible substance such as calcium, still a suitable threshold for production or release of this factor, coupled with decay and diffusion, could still produce a significant intracellular gradient. In any case, our results demonstrate that a cell can maintain an *intracellular* gradient in response to the extracellular signal during the time period in which cells are thought to determine their orientation.

Moreover, Fig. 15 demonstrates that if the cell uses an internal gradient mechanism for orientation, then a high-affinity mPDE certainly promotes reliable orientation by amplifying the front-to-back ratio.

5. Conclusion

The results presented here have significant implications for our understanding of amoeboid chemotaxis. Heretofore four basic mechanisms have been suggested: a spatial gradient sensing mechanism, a differential force mechanism, a ''pseudo-spatial'' mechanism and a

spatio-temporal threshold mechanism. Our results show that a spatial gradient sensing mechanism is inefficient in the presence of mPDE, since mPDE decreases the concentration difference between front and back. While we cannot preclude the "pseudo-spatial" mechanism, our results show that cells usually sense a significant concentration increase in all directions, which imposes a heavy burden on the sensitivity required for this mechanism. The problem is not how to distinguish directions in which the attractant is increasing from those in which it is decreasing, but rather to distinguish between more and less favorable directions.

Our results also show that the front-to-back cAMP ratio could be used to determine orientation, while the average over the cell of the time derivative of cAMP could be used to control the onset of movement. Concerning the former, it was shown that the front-to-back ratio of cAMP concentrations is increased significantly by the presence of mPDE, which could have a significant effect on the ability of a cell to orient. The latter is consistent with previous results (Dallon & Othmer, 1997), which showed that movement rules based on an intracellular "motion controller" that adapts to constant extracellular cAMP produces aggregation patterns very similar to what is observed. If in addition the duration is controlled by a substance that adapts to the extracellular cAMP signal, as was assumed in Dallon & Othmer (1997), then this rule automatically takes care of the "back-of-the-wave" problem (Soll *et al*., 1993). Furthermore, the presence of signal relay actually enhances the utility of this rule for initiating movement, since the time derivatives peak at about the time orientation is thought to be determined.

Thus we conclude that a spatio-temporal threshold mechanism, in which the spatial gradient of an intracellular factor is used for orientation, and the time derivative of cAMP is used to initiate movement, provides a feasible mechanism for extracting directional information and initiating movement during aggregation.

The authors are indebted to E. Pate, who participated in the development and analysis of an earlier unpublished version of the model developed here. This research was supported in part by NIH Grant GM # 29123 and ESPRC Grant GR/K71394.

REFERENCES

Berg, H. (1975). How bacteria swim. *Scient. Am.* **233,** 36–44.

Berg, H. C. & Brown, D. A. (1972). Chemotaxis in *Escherichia coli* analysed by three-dimensional tracking. *Nature* **239,** 500–504.

Bonner, J. T. (1982). Comparative biology of cellular slime molds. In: *The Development of* Dictyostelium discoideum (Loomis, W. F., ed.) pp. 1–33. London: Academic Press.

Brachet, P., Dicou, E. & Klein, C. (1979). Inhibition of cell differentiation in a phosphodiesterase defective mutant of *Dictyostelium discoideum*. *Cell Diff.* **8,** 255–265.

Brenner, M. & Thomas, S. D. (1984). Caffeine blocks activation of cyclic AMP synthesis in *Dictyostelium discoideum*. *Devel. Biol.* **101,** 136–146.

Brown, P. N. & Saad, Y. (1987) (November). Hybrid krylov methods for nonlinear systems of equations. Tech. rept. ucrl-97645. Lawrence Livermore National Laboratory.

Brundage, R. A., Fogarty, K. E. & Fay, F. S. (1991). Calcium gradients underlying polarization and chemotaxis of eosinophils. *Science* **254,** 703–706.

Cohen, M. H. & Robertson, A. (1971). Wave propagation in the early stages of aggregation of cellular slime molds. *J. theor. Biol.* **31,** 101–118.

Condeelis, J., Bresnick, A., Demma, M., Dharmawardhane, S., Eddy, R., Hall, A. L., Sauterer, R. & Warren, V. (1990). Mechanisms of amoeboid chemotaxis: an evaluation of the cortical expansion model. *Dev. Genetics* **11,** 333–340.

Dallon, J. C. (1996) (August). A mathematical study of chemotaxis in *Dictyostelium discoideum*. Ph.D. Thesis, University of Utah.

Dallon, J.C. & Othmer, H. G. (1997). A discrete cell model with adaptive signalling for aggregation of *Dictyostelium discoideum*. *Phil. Trans. R. Soc. Lond. Ser. B* **352,** 391–417.

Darmon, M., Barra, J. & Brachet, P. (1978). The role of phosphodiesterase in aggregation of *Dictyostelium discoideum*. *J. Cell Sci.* **31,** 233–243.

DeLisi, C. & Marchetti, F. (1982). A theory of measurement error and its implications for spatial and temporal gradient sensing during chemotaxis. *Cell Biophys.* **4,** 211–229.

Devreotes, P. N. & Steck, T. L. (1979). Cyclic 3′,5′ AMP relay in *Dictyostelium discoideum* II. Requirements for the initiation and termination of the response. *J. Cell Biol.* **80,** 300–309.

DeYoung, G., Monk, P. B. & Othmer, H. G. (1988). Pacemakers in aggregation fields of *Dictyostelium discoideum*. Does a single cell suffice? *J. Math. Biol.* **26,** 486–517.

Fisher, P., Merkl, R. & Gerisch, G. (1989). Quantitative analysis of cell motility and chemotaxis in *Dictyostelium*. *J. Cell Biol.* **92,** 807–821.

Futrelle, R., Traut, J. & McKee, W. G. (1982). Cell behavior in *Dictyostelium discoideum*: preaggregation

response to localized cyclic AMP pulses. *J. Cell Biol.* **92,** 807–821.

Gerisch, G. & Wick, U. (1975). Intracellular oscillations and release of cyclic AMP from *Dictyostelium* cells. *Biochem. Biophys. Res. Commun.* **65,** 364–370.

Gerisch, G., Hulser, D., Malchow, D. & Wick, U. (1975a). Cell communication by periodic cyclic amp pulses. *Phil. Trans. R. Soc. Lond.* **272,** 181–192.

Gerisch, G., Malchow, D., Huesgen, A., Nanjundiah, V., Roos, W. & Wick, U. (1975b). Cyclic AMP reception and cell recognition in *Dictyostelium discoideum*. In: *Developmental Biology icn-ucla Symposia on Molecular and Cellular Biology Vol.* 2 (McMahon, D. & Fox, C. F., eds), pp. 76–88. New York: NY: Benjamin.

Gilbert, S. H., Perry, K. & Fay, F. S. (1994). Mediation of chemoattractant-induced changes in (ca-2+)-i and cell shape, polarity, and locomotion by insp-3, dag, and protein kinase c in newt eosinophils. *J. Cell Biol.* **127,** 489–503.

Gingle, A.R. (1976). Critical density for relaying in *Dictyostelium discoideum* and its relation to phosphodiesterase secretion into the extracellular medium. *J. Cell Sci.* **20,** 1–20.

Gingle, A. R. & Robertson, A. (1976). The development of the relaying competence in *Dictyostelium discoideum*. *J. Cell Sci.* **20,** 21–27.

Glazer, P. M. & Newell, P. C. (1981). Initiation of aggregation by *Dictyostelium discoideum* in mutant populations lacking pulsatile signalling. *J. Gen. Microbiol.* **125,** 221–232.

Green, A. & Newell, P. (1975). Evidence for the existence of two types of CAMP binding sites in aggregating cells of *Dictyostelium discoideum*. *Biochem. J.* **140,** 313–322.

Höfer, T., Sherratt, J. A. & Maini, P. K. (1995). *Dictyostelium discoideum*: cellular self-organization in an excitable biological medium. *Proc. R. Soc. Lond. B* **259,** 249–257.

Killich, T., Plath, P. J., Wei, X., Bultmann, H., Rensing, L. & Vicker, M. G. (1993). The locomotion, shape and pseudopodial dynamics of unstimulated *Dictyostelium* cells are not random. *J. Cell Sci.* **106,** 1005–1013.

Konijn, T. M. & Raper, K. B. (1961). Cell aggregation in *Dictyostelium discoideum*. *Devel. Biol.* **3,** 725–756.

Kressin *et al.* (1979).

Kuwayama, H., Ishida, S. & Van Haastert, P. J. M. (1993). Nonchemotactic *Dictyostelium* mutants with altered cgmp signal transduction. *J. Cell Biol.* **123,** 1453–1462.

Levine, H. & Reynolds, W. (1991). Streaming instability of aggregating slime mold amoebae. *Phys. Rev. Letts.* **May,** 2400–2403.

MacKay, S. (1978). Computer simulation of aggregation in *Dictyostelium discoideum*. *J. Cell. Sci.* **33,** 1–16.

Malchow, D., Fuchida, J. & Nanjundiah, V. (1975). A plausible role for a membrane bound cAMP phosphodiesterase in cellular slime mold chemotaxis. *Biochem. Biophys. Acta* **385,** 421–428.

Martiel, J. L. & Goldbeter, A. (1987). A model based on receptor desensitization for cyclic AMP signaling in *Dictyostelium* cells. *Biophys. J.* **52,** 807–828.

Mato, J. M., Losada, A., Nanjundiah, V. & Konijn, T. M. (1975). Signal input for a chemotactic response in the cellular slime mold *Dictyostelium discoideum*. *Proc. Nat. Acad. Sci.* (*U.S.A.*) **72,** 4991–4993.

McRobbie, S. J. (1986). Chemotaxis and cell motility in the cellular slime molds. *Crit. Revs Microbiol.* **13**(4), 335–375.

Monk, P. B. & Othmer, H. G. (1989). Cyclic AMP oscillations in suspensions of *Dictyostelium discoideum*. *Phil. Trans. R. Soc. Lond.* **323,** 185–224.

Nanjundiah, V. & Malchow, D. (1976). A theoretical study of the effects of cyclic AMP phosphodiesterases during aggregation in *Dictyostelium*. *J. Cell Sci.* **22,** 49–58.

Newell, P. C. (1986). The role of actin polymerization in amoebal chemotaxis. *BioEssays* **5,** 202–212.

Oss, C. V., Panfilov, A., Hogeweg, P., Siegert, F. & Weijer, C. (1996). Spatial pattern formation during aggregation of the slime mould *Dictyostelium discoideum*. *J. theor. Biol.* **181,** 203–213.

Othmer, H. G. & Pate, E. F. (1987). A model for pattern formation in *Dictyostelium discoideum*. In: *Mathematical Topics in Population Biology, Morphogenesis, and Neurosciences* (Teramoto, E. & Yamaguti, M., eds), pp. 224–233. Berlin: Springer-Verlag.

Othmer, H. G. & Schaap, P. (1997). *The role of cAMP in the development of* Dictyostelium discoideum. *Comm. Theor. Biol.* (to appear).

Parnas, H. & Segel, L. A. (1977). Computer evidence concerning the chemotactic signal in *Dictyostelium discoideum*. *J. Cell Sci.* **25,** 191–204.

Pate, E. & Odell, G. (1981). A computer simulation of chemical signaling during the aggregation phase of *Dictyostelium discoideum*. *J. theor. Biol.* **88,** 201–239.

Pate, E. & Othmer, H. G. (1986). Differentiation, cell sorting and proportion regulation in the slug stage of *Dictyostelium discoideum*. *J. theor. Biol.* **118,** 301–319.

Pate, E. F., Elwood, D. & Othmer, H. G. (1988). mPDE dramatically affects cAMP levels near aggregating *D. Dictyostelium* cells. (unpublished).

Peaceman, D. W. & Rachford, Jr., H. H. (1955). The numerical solution of parbolic and elliptic differential equations. *J. Soc. Indust. Appl. Math.* **3**(1), 28–41.

Raman, R. K., Hashimoto, Y., Cohen, M. H. & Robertson, A. (1976). Differentiation for aggregation in the cellular slime molds: the emergence of autonomously signalling cells in *Dictyostelium discoideum*. *J. Cell Sci.* **21,** 243–259.

Roos, W., Nanjundiah, V., Malchow, D. & Gerisch, G. (1975). Amplification of cyclic AMP signals in aggregating cells of *Dictyostelium discoideum*. *FEBS Letts.* **53,** 139–142.

Ross, F. M. & Newell, P. C. (1981). Streamers: chemotactic mutants of *Dictyostelium discoideum* with altered cyclic gmp metabolism. *J. Gen. Microbiol.* **127,** 339–350.

Rossier, C., Eitle, E., Van Drievl, R. & Gerisch, G. (1980). Biochemical regulation of cell development and aggregation in *Dictyostelium discoideum*. In: *Symposium of the Society for General Microbiology* (Gooday, G. W., Lloyd, D. & Trinci, A. P. J., eds), pp. 405–427. Cambridge: Cambridge University Press, for Society for General Microbiology.

Savill, N. & Hogeweg, P. (1997). Modelling morphogenesis: from single cells to crawling slugs. *J. theor. Biol.* **184,** 229–235.

Shenderov, A. & Sheetz, M. (1997). Inversely correlated cycles in speed and turning in an ameba: an oscillatory model of cell locomotion. *Biophys. J.* **72**(5), 2382–2389.

Siegert, F. & Weijer, C. J. (1989). Digital image processing of optical density wave propagation in *Dictyostelium discoideum* and analysis of the effects of caffeine and ammonia. *J. Cell Sci.* **93,** 325–335.

Soll, D. R., Wessels, D. & Sylwester, A. (1993). The motile behavior of amoebae in the aggregation wave in *Dictyostelium discoideum*. In: *Experimental and Theoretical Advances in Biological Pattern Formation*. (Othmer, H. G., Maini, P. K. & Murray, J. D., eds), London: Plenum.

Spiro, P. A., Parkinson, J. S. & Othmer, H. G. (1997). A model of excitation and adaptation in bacterial chemotaxis. *Proc. Nat. Acad. Sci. (U.S.A.)* **94,** 7263–7268.

Swanson, J. & Taylor, D. L. (1982). Local and spatially coordinated movements in *Dictyostelium discoideum* amoebae during chemotaxis. *Cell* **28,** 225–232.

Tang, Y. & Othmer, H. G. (1994). A G-protein-based model of adaptation in *Dictyostelium discoideum*. *Math. Biosci.* **120,** 25–76.

Tang, Y. & Othmer, H. G. (1995). Excitation, oscillations and wave propagation in a G-protein based model of signal transduction in *Dictyostelium discoideum*. *Phil. Trans. R. Soc. (Lond)* **B349,** 179–195.

Tomchik, K. J. & Devreotes, P. N. (1981). Adenosine 3′,5′-monophosphate waves in *Dictyostelium discoideum*: a demonstration by isotope dilution-fluorography. *Science* **212,** 443–446.

Tranquillo, R. & Lauffenburger, D. (1987). Stochastic models of chemosensory cell movement. *J. Math. Biol.* **25,** chemotaxis.

Tranquillo, R. T. & Alt, W. (1994). Dynamic morphology of leukocytes: statistical analysis and a stochastic model for receptor-mediated cell motion and orientation. In: *Biomechanics of Active Motion and Division of Cells* (Akkas, N., ed.), pp. 437–443. Berlin: Springer-Verlag.

Valkema, R. & Haastert, P. J. M. V. (1994). A model for cAMP-mediated cGMP response in *Dictyostelium discoideum*. *Mol. Biol. Cell* **5** (May), 575–585.

Van Duijn, B. & Van Haastert, P. J. M. (1992). Independent control of locomotion and orientation during *Dictyostelium discoideum* chemotaxis. *J. Cell Sci.* **102,** 763–768.

Van Haastert, P. & Van der Heijden, P. (1983). Excitation, adaptation, and deadaptation of the cAMP-mediate d cGMP response in *Dictyostelium discoideum*. *J. Cell Biol.* **96,** 347–353.

Varnum, B., Edwards, K. B. & Soll, D. R. (1985). *Dictyostelium* amebae alter motility differently in response to increasing versus decreasing gradients of cAMP. *J. Cell Biol.* **101,** 1–5.

Vasiev, B. N., Hogeweg, P. & Pantifilov, A. V. (1994). Simulation of *Dictyostelium discoideum* aggregation via reaction-diffusion model. *Phys. Rev. Letts.* **73,** 3173–3176.

Vasieva, O. O., Vasiev, B. N., Karpov, V. A. & Zaikin, A. N. (1994). A model of *Dictyostelium* aggregation. *J. theor. Biol.* **171,** 361–367.

Vicker, M. G. (1994). The regulation of chemotaxis and chemokinesis in *Dictyostelium* amoebae by temporal signals and spatial gradients of cyclic amp. *J. Cell Sci.* **107**(2), 659–667.

Wessels, D., Murray, J. & Soll, D. R. (1992). Behavior of *Dictyostelium* amoebae is regulated primarily by the temporal dynamic of the natural cAMP wave. *Cell Motility Cytoskeleton* **23**(2), 145–156.

Zigmond, S. H. (1978). Chemotaxis by polymorphonuclear leukocytes. *J. Cell Biol.* **77,** 269–287.

APPENDIX

Description of the Numerical Methods and their Implementation

In this Appendix the numerical methods used to solve the model as well as the implementational details of the scheme are explained. We begin with the methods used for the exterior eqn (6) and the associated boundary conditions given in eqns (7), then proceed to the methods used for the interior eqns (11) and (12) and finish with how the interior and exterior equations are linked via boundary values.

NUMERICAL METHODS FOR THE EXTERIOR EQUATIONS

The exterior equation consists of a parabolic equation

$$\frac{\partial \bar{u}}{\partial y} = D\Delta\bar{u} + F(\bar{u}) \text{ on } R^2 - (\Omega_1 \cup \Omega_2) \quad \text{(A.1)}$$

where D is the diffusion constant, Δ is the Laplace operator in two space dimensions, F is a continuous function and Ω_1 and Ω_2 are discs representing the cells. The two cell membranes create the boundaries, and their associated fluxes determine the boundary conditions. They are written as

$$D\frac{\partial \bar{u}}{\partial n_1} = f_1(\bar{u}, t) \text{ on } \partial\Omega_1$$

$$D\frac{\partial \bar{u}}{\partial n_2} = f_2(\bar{u}, t) \text{ on } \partial\Omega_2. \quad \text{(A.2)}$$

The domain, the plane minus the two discs, is conformally mapped to an annulus with inner radius r_0 and outer radius 1 (see Fig. A1).

The conformal map is defined by

$$w = \frac{z - a}{az - 1}$$

where $z = x_1 + ix_2$ is a point in the complex plane and

$$a = \frac{1 + x_1x_2\sqrt{(x_1^2 - 1)(x_2^2 - 1)}}{x_1 + x_2}, \quad \text{(A.3)}$$

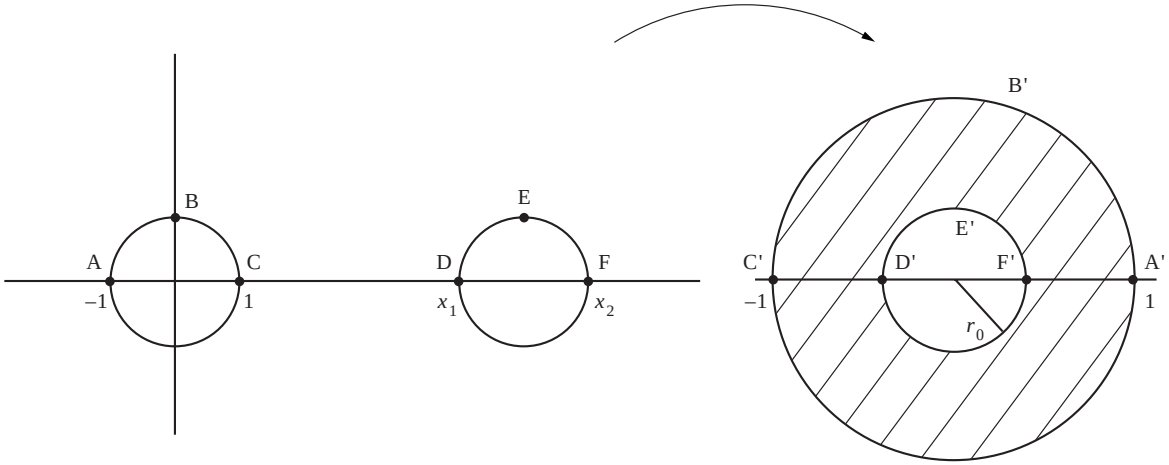

FIG. A1. The original exterior domain and how it is changed via the conformal mapping. The labeled points are transformed to the correspondingly labeled points (i.e. A is transformed to A′).

maps the plane into the annulus with outer radius 1 and inner radius r_0 defined by

$$r_0 = \frac{x_1 x_2 - 1 - \sqrt{(x_1^2 - 1)(x_2^2 - 1)}}{x_2 - x_1}. \quad \text{(A.4)}$$

The Cartesian coordinates are changed to polar coordinates and in order to prevent the grid points, in the original domain of the plane, from being clustered around the signaling cell and sparsely placed near the receiving cell (see Fig. A2) we make one further transformation defined by

$$\rho = \ln\left(\frac{r}{r_0}\right) + r_0. \quad \text{(A.5)}$$

Thus the problem to be solved numerically has the following form:

$$\frac{\partial u}{\partial t} = Lu + Hu \quad \text{(A.6)}$$

$$Lu = G(r, \theta)\left[\frac{\partial^2 u}{\partial \rho^2}\left(\frac{\partial \rho}{\partial r}\right)^2 + \frac{\partial u}{\partial \rho}\left(\frac{\partial^2 \rho}{\partial r^2}\right) + \frac{1}{r}\frac{\partial u}{\partial \rho}\left(\frac{\partial \rho}{\partial r}\right) + \frac{1}{r^2}\frac{\partial^2 u}{\partial \theta^2}\right] \quad \text{(A.7)}$$

$$Hu = F(u) \quad \text{(A.8)}$$

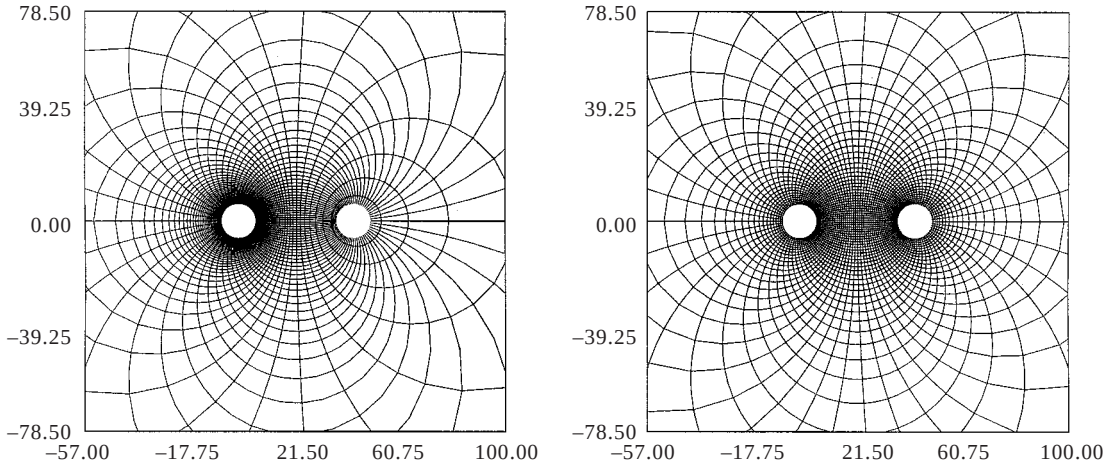

FIG. A2. The grid lines are shown when mapped to the plane. In (a) a uniform grid on the annulus is mapped to the plane. The grid used in the simulations is shown in (b) where a non-uniform radial grid on the annulus is mapped to the plane. Every other radial grid line is printed in both figures.

with outer boundary conditions as

$$\frac{\partial u}{\partial \rho}(\rho(1), \theta, t) = g_2(u, t) \tag{A.9}$$

$$g_2(u, t) = \frac{1}{D}\frac{\partial r}{\partial \rho}\left|\frac{\mathrm{d}z}{\mathrm{d}w}\right|_{r=1} f_2(u, t), \tag{A.10}$$

with inner boundary conditions as

$$\frac{\partial u}{\partial \rho}(r_0, \theta, t) = g_1(u, t) \tag{A.11}$$

$$g_1(u, t) = -\frac{1}{D}\frac{\partial r}{\partial \rho}\left|\frac{\mathrm{d}z}{\mathrm{d}w}\right|_{r=r_0} f_1(u, t), \tag{A.12}$$

and with the periodic boundary conditions

$$u(\rho,0, t) = u(\rho,2\pi, t), \tag{A.13}$$

where

$$G(r, \theta) = \frac{D(a^2r^2 - 2ar\cos\theta + 1)^2}{(a^2 - 1)^2} \tag{A.14}$$

and

$$\left|\frac{\mathrm{d}z}{\mathrm{d}w}\right| = \frac{a^2 - 1}{a^2r^2 - 2ar\cos\theta + 1}. \tag{A.15}$$

Here $u(\rho, \theta) = \bar{u}(x, y)$, a and z are defined above and w is the variable in the range of the conformal mapping.

The numerical scheme used is based on the Alternating Direction Implicit method (Peaceman & Rachford, 1955). With the following discretized equations

$$\left[1 - \frac{kG}{2h_\rho^2}\left(\frac{\partial \rho}{\partial r}\right)^2\delta_\rho^2 - \frac{kG}{4h_\rho}\left(\frac{\partial^2 \rho}{\partial r^2} + \frac{1}{r}\right)\delta_\rho\right]u_{\ell,m}^{n+1*} = \left[1 + \frac{kG}{2r^2h_\theta^2}\delta_\theta^2 + \frac{k}{2}H\right]u_{\ell,m}^{n} \tag{A.16}$$

$$\left[1 - \frac{kG}{2r^2h_\theta^2}\delta_\theta^2\right]u_{\ell,m}^{n+1} - \frac{k}{2}Hu_{\ell,m}^{n} = \left[1 + \frac{kG}{2h_\rho^2}\left(\frac{\partial \rho}{\partial r}\right)^2\delta_\rho^2 + \frac{kG}{4h_\rho}\left(\frac{\partial^2 \rho}{\partial r^2} + \frac{1}{r}\right)\delta_\rho\right]u_{\ell,m}^{n+1*} \tag{A.17}$$

where δ_ρ and δ_θ are the standard centered difference operators, $u_{l,m}^n = u(r_0 + (\ell - 1)h_\rho, (m - 1)h_\theta, nk)$, h_ρ is the step size in the ρ directions, h_θ is the step size in the θ directions and k is the time step. By time lagging the boundary conditions we have a linear system which is solved exactly.

NUMERICAL METHODS FOR THE INTERIOR EQUATIONS

The interior equations are of the following type

$$\frac{\partial v}{\partial t} = D\Delta v + F_1(v) \tag{A.18}$$

where v is a function of two space variables and time, and Δ is the Laplace operator in polar coordinates. The domain of eqn (A.18) is a disc of units r_0. The boundary conditions are

$$\frac{\partial v}{\partial r}(r_0, \theta, t) = f_1(v,\mathbf{v}) \tag{A.19}$$

$$\frac{\mathrm{d}\mathbf{v}}{\mathrm{d}t} = F_2(u, v,\mathbf{v}) \tag{A.20}$$

where u is a solution to eqn (A.6) and $\mathbf{v}$ is a three vector whose components are functions of one space variable and time. If we let k_i be the time step, h_{r_i} the radial step, h_{θ_i} the angular step, and

$$v(\ell h_{r_i}, mh_{\theta_i}, nk_i) = v_{\ell,m}^n \tag{A.21}$$

then the following equations describe the numerical scheme used for solving eqn (A.18)

$$\begin{aligned}\frac{v_{\ell,m}^{n+1} - v_{\ell,m}^n}{k_i} &= \frac{D}{2(h_{r_i})^2}(v_{\ell+1,m}^{n+1} - 2v_{\ell,m}^{n+1} + v_{\ell-1,m}^{n+1} + v_{\ell+1,m}^n - 2v_{\ell,m}^n + v_{\ell+1,m}^n) \\ &+ \frac{D}{4rh_{r_i}}(v_{\ell+1,m}^{n+1} - v_{\ell-1,m}^{n+1} + v_{\ell+1,m}^n - v_{\ell-1,m}^n) \\ &+ \frac{D}{2(h_{\theta_i})^2r^2}(v_{\ell,m+1}^{n+1} - 2v_{\ell,m}^{n+1} + v_{\ell,m-1}^{n+1} \\ &+ v_{\ell,m+1}^n - 2v_{\ell,m}^n + v_{\ell,m-1}^n) + F_1\left(\frac{v_{\ell,m}^{n+1} + v_{\ell,m}^n}{2}\right)\end{aligned}$$

where $i = 1$ denotes one cell and $i = 2$ denotes the other cell. The boundary condition in eqn (A.20) is solved using the midpoint rule

$$\frac{\mathbf{v}_{\ell,m}^{n+1} - \mathbf{v}_{\ell,m}^n}{k_i} = F_2\left(u, \frac{v_{\ell,m}^{n+1} + v_{\ell,m}^n}{2}, \frac{\mathbf{v}_{\ell,m}^{n+1} + \mathbf{v}_{\ell,m}^n}{2}\right).$$

The software package NKSOL (Brown & Saad, 1987) is used to solve the discretized equations by using hybrid krylov methods.

LINKING THE INTERIOR AND EXTERIOR EQUATIONS

Let Ω be the exterior domain, C_i be the interior domain for the i-th cell, and let B_i be the boundary between Ω and C_i where $i = 1, 2$. The time steps must satisfy $k = j_i k_i$ where j_i is a positive integer. Let v and $\mathbf{v}$ be solutions to eqns (A.18), (A.19) and (A.20) with domain C_1 and likewise $\bar{v}$ and $\bar{\mathbf{v}}$ for C_2.

The boundary conditions are implemented in the numerical scheme for the exterior equations in the following manner:

$$u_{0,m}^{n+1^*} = u_{2,m}^{n+1^*} - 2h_r[D(u^{n^*})u^{n+1^*} + f(v^n)] \quad \text{(A.22)}$$

$$u_{L+1,m}^{n+1^*} = u_{L-1,m}^{n+1^*} + 2h_r[D(u^{n^*})u^{n+1^*} + f(\bar{v}^n)]. \quad \text{(A.23)}$$

Let $v^{n,v} = v(r, \theta, nk + vk_i)$, $v^{n,j_i} = v^{n+1,0}$ and $v = 0, 1, 2, \ldots, j_i - 1$. In the interior equations the boundary conditions are implemented as (the following equations are valid for the barred variables as well with $i = 2$):

$$v_{L_i+1,m}^n = v_{L_i-1,m}^n + 2h_r f_1\left(\frac{v^n + v^{n-1}}{2}, \frac{\mathbf{v}^n + \mathbf{v}^{n-1}}{2}\right)$$

$$\mathbf{v}^{n,v+1} - \mathbf{v}^{n,v} =$$

$$k_i\left[(1-\Theta)F_2(u^{n+1}, \frac{v^{n,v+1} + v^{n,v}}{2}, \frac{\mathbf{v}^{n,v+1} + \mathbf{v}^{n,v}}{2}\right)$$

$$+\Theta F_2\left(u^n, \frac{v^{n,v+1} + v^{n,v}}{2}, \frac{\mathbf{v}^{n,v+1} + \mathbf{v}^{n,v}}{2}\right)\Big]$$

where

$$\Theta = 1 + \frac{1}{2j_i} - \frac{v+1}{j_i} \quad \text{(A.24)}$$

and $i = 1$. Unless stated otherwise all simulations have a discretization for the exterior domain with 75 angular points, 100 radial points and a time step of 2×10^{-4} minutes. When the interior dynamics are added the time step is decreased to 2×10^{-6} minutes. The interior discretization has 20 angular points, 10 radial points and $j \leqslant 4$.